Received: 15 January 2021 | Revised: 27 May 2021 | Accepted: 28 May 2021

DOI: 10.1002/eqe.3503

RESEARCH ARTICLE

WILEY

Evaluation of seismic performance of as-built and retrofitted reinforced concrete frame structures with LAP splice deficiencies

Eyitayo A. Opabola[1] | **Kenneth J. Elwood**[2] | **Abbie B. Liel**[3]

[1] Department of Civil, Environmental and Geomatic Engineering, University College London, London, United Kingdom

[2] Department of Civil and Environmental Engineering, University of Auckland, Auckland, New Zealand

[3] Department of Civil, Environmental and Architectural Engineering, University of Colorado, Boulder, USA

Correspondence
Eyitayo A. Opabola, Department of Civil, Environmental and Geomatic Engineering, University College London, London, United Kingdom.
Email: e.opabola@ucl.ac.uk

Abstract

Several studies have looked at the development of hinge models to simulate the hysteretic response of flexure- and shear-critical reinforced concrete (RC) beam-column components from damage initiation to onset of gravity collapse. However, few studies have been conducted to develop similar models for older type bond-critical beam-column components. First, using existing experimental data, this paper describes the calibration of simple and efficient hinge models to simulate the inelastic hysteretic response of as-built and retrofitted splice-deficient columns. Subsequently, to demonstrate the applicability of the hinge models, the seismic performance of as-built and fibre-reinforced polymer (FRP) -retrofitted two- and four-story nonductile RC frame buildings with splice-deficient columns are assessed using nonlinear dynamic analysis procedures. The results show that buildings with bond-critical columns may have a lower collapse potential than buildings with shear-critical columns, implying that in certain cases a longer splice length may actually worsen performance. According to the analyses, local retrofitting of the columns can significantly improve the seismic performance of the buildings. Contrary to results presented in this study, a significant U.S. evaluation methodology for RC frame buildings, FEMA P-2018, indicates that buildings with bond-critical columns have similar collapse potential as buildings with shear-critical columns. Modifications are proposed to improve the FEMA P-2018 provisions. The modelling approach presented in this paper are recommended for incorporation into ASCE/SEI 41, engineering practice and future research.

KEYWORDS

bond-critical, collapse fragility, hinge models, lap splice, nonductile buildings, nonlinear analysis, retrofitted structures, seismic performance

1 | INTRODUCTION

Several design and detailing deficiencies have contributed to the poor performance of older reinforced concrete (RC) buildings in past earthquakes.[1–3] In particular, there is concern about the progressive loss of the gravity-load-bearing

capacity of the poorly detailed RC columns in these buildings. Relative to other buildings, these structures are classified as collapse-prone and, therefore, a high priority for evaluation and retrofit.

Despite the "collapse-prone" tag attached to pre-1980s RC structures, reconnaissance data have shown that only a relatively small proportion of these buildings have collapsed in past earthquakes. Otani[4] used data from four strong seismic events with magnitude M ≥ 6.7 to show that a significant number of pre-1980s buildings suffered operational (i.e., light to moderate) damage following strong earthquake shaking, while only about 2–10% of buildings suffered partial or total collapse. Likewise, despite the presence of several pre-1980s structures in the Christchurch (New Zealand) region, only one pre-1980s building collapsed following the 2010/2011 Canterbury earthquakes.[5] Instead of classifying all pre-1980s buildings as collapse-prone, it is important to identify the buildings with the highest collapse risk, such that they can be prioritised for risk mitigation efforts to improve overall community resilience.

As a step towards risk mitigation, seismic assessment procedures have been developed to assess the response of these older type structures at the component and global levels. Owing to a lack of sufficient knowledge on the seismic response of RC frame structures on the global and component level, codified seismic assessment provisions in seismically active regions, for example, the United States[6] and New Zealand,[7] can be inherently conservative leading to potentially unwarranted retrofits or potentially building closures[8]; this conservatism can pose a significant financial burden on the global economy and lead to poor prioritisation of those buildings that most threaten community seismic resilience. With the aim of tackling these problems, FEMA developed guidelines for identifying older RC buildings with high collapse potential (see FEMA P-2018[9]).

Prior to the 1980s, RC design codes allowed the presence of inadequate splices in the plastic hinge regions of RC columns; hence, it is not uncommon to have a significant number of buildings with inadequate column splice detailing. Experimental studies[10–12] have demonstrated that the response of RC columns with short splices (a term we use interchangeably with splice-deficient columns) may be significantly different from that of columns with continuous reinforcement. The response of columns with short splices is expected to have an influence on the global response of the structure, especially if a weak column-strong beam mechanism is prevalent. However, many efforts[13,14] focusing on modelling and collapse assessment of RC buildings have not accounted for these effects and there is uncertainty as to how best to represent the force–displacement response of components with short splices.[15]

State-of-the-art seismic assessment procedures (e.g., ASCE/SEI 41–17, FEMA P-2018[9], Eurocode 8–3[16]) adopt varying approaches for the seismic assessment of columns with short splices. Following the ASCE/SEI 41-17 procedure, the majority of columns with short splices in the plastic hinge region will be classified as bond-critical (defined in ASCE/SEI 41-17 as columns controlled by inadequate development or splicing). ASCE/SEI 41-17 provides a formulation tailored for evaluating the response of columns classified as bond-critical. On the other hand, FEMA P-2018 provisions assume that all columns with short splices can be treated as columns with continuous reinforcement (in terms of deformation capacity). To account for a reduced deformation capacity at lateral failure in columns with provided splice length (l_o) shorter than the 'minimum required lap length for the column to develop its full ultimate deformation capacity as if its bars were continuous ($l_{ou,min}$)', Eurocode 8-3 recommends that the full deformation capacity be multiplied $l_o/l_{ou,min}$. It is noteworthy that compared to ASCE/SEI 41-17, Eurocode 8-3 does not make provisions for evaluating the deformation capacity at the axial failure of concrete columns.

Experimental results have shown that columns with short splices in the plastic hinge region may experience bond-critical, flexure-shear or brittle shear-critical failure modes depending on detailing and boundary conditions. A review of these experimental studies[17] has shown that the seismic behaviour of RC columns with short splices is significantly influenced by the failure mode. Hence, fragility estimates based on ASCE/SEI 41-17, and FEMA P-2018 provisions, which do not appropriately account for failure mode effects, may not be representative of the actual fragility of RC frames with splice-deficient columns.

In this paper, using experimental data from various studies, simple and efficient hinge models are calibrated to simulate the inelastic hysteretic response of as-built and FRP-retrofitted columns with short splices. Subsequently, the proposed models are adopted in evaluating the seismic performance of two- and four-story archetype buildings designed to the 1967 Uniform Building Code[18] through nonlinear dynamic analyses. For each archetype building set, three different structures were considered – a structure with shear-critical columns, a structure with bond-critical columns and a structure with FRP-retrofitted columns – for a total of six frames. The seismic fragility of the structures at four limit states (immediate occupancy [IO], life safety [LS], collapse prevention [CP] and global collapse) were evaluated. Results show the impact of column detailing vulnerabilities and retrofit on the seismic performance of older type RC frame structures. Furthermore, the collapse potential of each building was evaluated using the FEMA P-2018 methodology. Subsequently, recommendations are proposed for improving the FEMA P-2018 methodology for assessing buildings with splice-deficient columns.

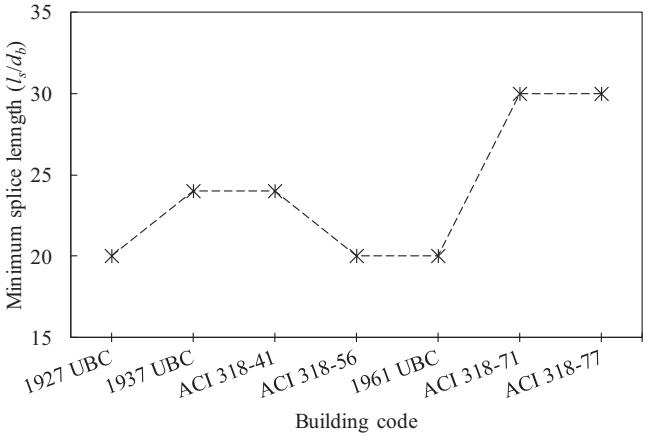

FIGURE 1 Minimum lap-splice length requirements of pre-1980s building codes

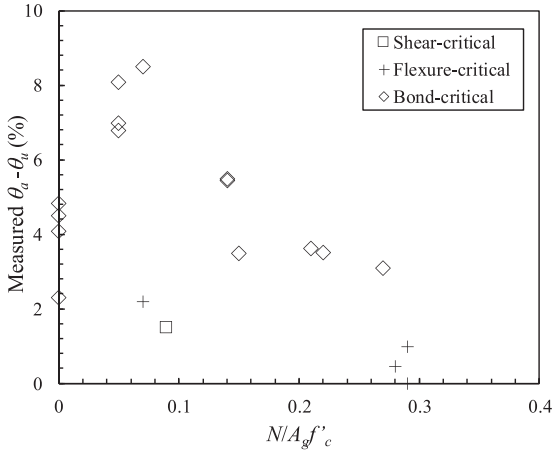

FIGURE 2 Influence of failure mode and axial load ratio on the buffer between drifts at lateral failure (θ_u) and axial failure (θ_a) in columns with lap splice deficiencies (data available in Opabola and Elwood[17])

2 | RESPONSE OF COLUMNS WITH SHORT SPLICES IN THE PLASTIC HINGE REGION

Older RC design codes[19–22] allowed for splice length between $20d_b$ and $30d_b$ to be provided in the plastic hinge region of RC columns (see Figure 1). Modern design codes[23,24] recommend that splices should be located away from the regions of maximum moment demands. Aside from allowing short lap splices, older codes allowed the use of poorly anchored and widely spaced transverse reinforcement in the plastic hinge regions of RC columns. Hence, these columns are susceptible to brittle failure mechanisms.

To assess the response of columns with short splices in plastic hinge regions, a number of experimental programs[10,25] have been carried out on column specimens considering various governing parameters – axial load level, splice length, stirrup spacing and loading protocol. A summary of test data on columns with short straight splices is available in Opabola and Elwood.[17] Based on available experimental data, three distinct failure modes have been observed – brittle-shear, flexure-shear and bond-critical failure modes. Similar to columns with continuous reinforcement, the response of brittle-shear and flexure-shear critical columns with short splices is characterised by failure through a diagonal plane (with the distinction depending on whether this occurs before or after flexural yielding). In these failure modes, following the development of the critical diagonal failure plane, an axial load is resisted through a shear-friction mechanism along the diagonal plane.[26]

Experimental results in Figure 2 show that, as a result of the brittle nature of the shear-friction mechanism, loss of vertical load-carrying capacity typically occurs shortly after lateral failure – with a buffer of typically less than 1.5% drift. However, according to experimental data,[10] fixed-end rotation accounts for up to 90% of total rotation in bond-critical

columns, i.e., bond-critical columns are dominated by a rocking mechanism. Due to the pseudo-ductile nature of the rocking mechanism of bond-critical columns, these columns tend to have a larger buffer between lateral failure (defined as 20% drop in lateral resistance) and axial failure (See Figure 2). In some of the reported test programs, no axial failure was in fact reported at drift levels above 7%. It is noteworthy that state-of-the-practice seismic assessment provisions[6,9,16] do not recognise the large buffer between lateral and axial failure in bond-critical columns. Hence, there is little or no information on how this large buffer affects the global seismic performance and collapse fragility of RC frame structures.

3 | MODELLING OF AS-BUILT AND RETROFITTED COLUMNS WITH SHORT SPLICES

3.1 | Existing approaches for modelling columns with short splices

The focus here is on macro-modelling approaches suitable for nonlinear response history analysis procedures in seismic assessment guidelines. Among these, Cho and Pincheira[27] proposed a macro-modelling approach for modelling the response of columns with short splices. The model consists of an elastic beam-column element with three zero-length springs – a nonlinear rotational spring to capture flexural deformation, a nonlinear shear spring to capture shear deformation and a nonlinear rotational bond-slip spring to capture the bond-slip deformation. The moment-slip rotation relationship of the bond-slip zero-length spring is calibrated by combining results from two analyses. Firstly, the uniaxial pull-out force versus uniaxial slip deformation is estimated using a one-dimensional analysis on an isolated reinforcing bar embedded in concrete. Then, a moment-curvature analysis is carried out to relate the pull-out force to the moment applied to the critical section of the column. Furthermore, the slip rotation is computed by dividing the estimated uniaxial slip deformation, obtained from the one-dimensional analysis on an isolated reinforcing bar embedded in concrete, by the difference between the effective depth and neutral axis depth obtained from the moment-curvature analysis.

The major disadvantage of the Cho and Pincheira[27] approach is that it requires multiple steps in the analysis of the column element which can be time-consuming. Furthermore, the moment-curvature analysis is based on an assumption of concrete-rebar deformation compatibility – an assumption that may not be valid once bond degradation has occurred. Also, as pointed out by Chowdhury and Orakcal,[28] using predefined loading and unloading rules for the bond-slip spring tends to introduce incompatibility between the bond-slip and flexural deformations, compromising the reliability of this type of approach.

ASCE/SEI 41-17 recommends modelling parameters for predicting the inelastic response of bond-critical columns. These modelling parameters for bond-critical columns were derived from regression analyses on a database of columns with short splices which included shear-critical columns with short splices.[15] Analytical studies[17] have shown that the ASCE/SEI 41-17 provisions are significantly conservative. Hence, hinge models using the ASCE/SEI 41-17 modelling parameters may not adequately capture the inelastic hysteretic response of bond-critical columns.

A number of other macro- and micro-modelling approaches have also been proposed by other researchers.[28,29] Aside from the complexities in the definition and implementation of these models, there are also difficulties in achieving numerical convergence under cyclic loading. There is also evidence that, despite the complexities of these models, they may be unable to capture the potential post-yield flexure-shear interaction as observed in experimental tests.[25,30]

3.2 | Proposed approach

A failure mode-based modelling approach is adopted in this section. The adopted approach is based on the well-established knowledge that the contribution of deformation components (i.e. flexure, shear and bar slip) to total deformation is dependent on failure mode; such that, for effective and efficient modelling, it is appropriate to first identify the probable failure mode of the column. The failure mode of a column with a short splice can be evaluated using the strength-based procedure.[17] In this strength-based procedure, the probable flexural strength, the lateral strength corresponding to maximum developable tensile stress in the splice, and the undegraded shear strength are compared. As presented in Opabola and Elwood,[17] the adequacy of the strength-based approach was validated using a database of 29 columns with short splices, achieving a 93% accuracy in predicting the observed failure mode. Interested readers are referred to Opabola and Elwood[17] for more information. Once the probable failure mode is determined, the column can be modelled as presented below.

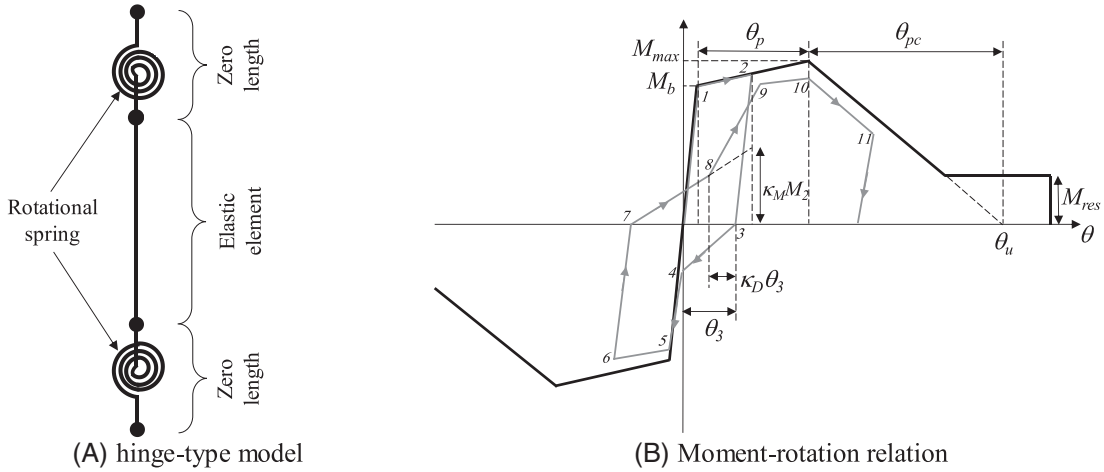

FIGURE 3 Proposed model for bond-critical columns (NB: The moment corresponding to the maximum developable tensile stress M_b is replaced by the yield moment M_y in components that experience flexural yielding, i.e., well-detailed or retrofitted column): (A) hinge-type model and (B) moment-rotation relation

3.2.1 | Modelling bond-critical columns

Based on experimental data,[10] the fixed-end rotation component contributes about 90% of the inelastic deformation of bond-critical columns. Hence, this study explores a lumped plasticity modelling approach for modelling the response of bond-critical columns. In the proposed approach, the column model consists of an elastic beam-column element and zero-length nonlinear rotational spring elements which models the bond degradation and rocking phases of the column (see Figure 3A).

The moment-rotation relationship of the nonlinear rotational spring is modelled using the modified Ibarra–Medina–Krawinkler (IMK) uniaxial material model[31] incorporated in OpenSees,[32] the software platform adopted for this study. In this model, the response of the column is idealised as a trilinear moment-rotation backbone. The key backbone parameters are the effective stiffness (EI_{eff}), moment corresponding to the maximum developable tensile stress (M_b), peak moment strength (M_{max}), pre-capping rotation capacity (θ_p), post-capping rotation capacity (θ_{pc}), ultimate rotation capacity (θ_u) and the residual strength capacity (M_{res}) (see Figure 3B). In addition, a number of hysteretic parameters are used to capture cyclic strength and stiffness deterioration (Λ) and pinching behaviour (κ). The definitions of these parameters are described below.

Effective stiffness (EI_{eff})

The effective stiffness is defined as the secant stiffness to the strength corresponding to the maximum developable tensile stress in the splice (i.e., M_b). Various recommendations[6,16,33–35] have been proposed to predict the effective stiffness of RC beam-column components. In this study, we adopt the Opabola and Elwood[35] formulation (Equation 1). To account for the contribution of bar slip and shear deformation components, Opabola and Elwood[35] proposed a modifier to the flexural rigidity coefficients of ASCE/SEI 41-17 as a function of aspect ratio (a/d). Equation (1) recognises that the contribution of bar slip and shear deformations to the elastic response is negligible in slender columns. For a database of 29 columns with short splices, Equation (1) provides an effective stiffness estimate with a mean ratio of observed to calculated of 1.0 and coefficient of variation (CoV) of 23.7%.[17]

$$\frac{EI_{eff}}{EI_g} = \alpha\left(0.27\left(\frac{a}{d}\right) - 0.07\right) \leq \alpha \tag{1}$$

where the effective stiffness coefficient from ASCE/SEI 41 (α) is the flexural rigidity coefficient from ASCE/SEI 41–17[6] and taken as 0.3 for axial load ratio $N/A_g f'_c \leq 0.1$, $\alpha = 0.7\, N/A_g f'_c \geq 0.5$ and linear interpolation for $0.1 < N/A_g f'_c < 0.5$; a/d is the aspect ratio of the column.

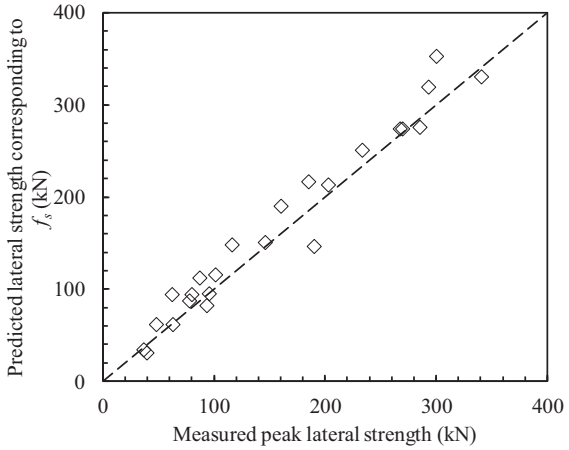

FIGURE 4 Comparison of measured peak strength to the computed lateral strength corresponding to maximum developable tensile stress f_s for bond-critical columns (data available in Opabola and Elwood[17])

Peak strength

In bond-critical columns, bond failure is initiated once the maximum developable tensile stress f_s is reached in the tensile bars. This corresponds to column moment capacity M_b . Typically, M_b is an output of the earlier mentioned strength-based failure mode classification procedure for columns with short splices. Given that longitudinal reinforcement yielding and strain hardening do not occur in bond-critical columns, the plateau in the moment-rotation can be assumed to be flat, i.e., M_{max}/M_b equals unity. As shown in Figure 4, the computed lateral strength corresponding to maximum developable tensile stress provides a good estimate of the measured peak strength of bond-critical columns with a mean measured-to-predicted ratio of 0.95 and CoV of 14.5%.

Pre-capping rotation capacity (θ_p)

Experimental results[10,11] have shown that, once bond failure is initiated, increased lateral drift demands will make the lap splices in the plastic hinge region progressively unzip along the provided splice length leading to significant concrete-rebar bond degradation. The progressive unzipping of the lap splice, together with the onset of damage to the concrete in the compression zone, leads to lateral failure of bond-critical columns.

Opabola and Elwood[17] proposed a mechanistic formulation (Equation 2) for evaluating the inelastic rotation capacity at lateral failure (θ_p) of bond-critical columns with short splices. The key assumption of the formulation is that the plastic deformation capacity of a bond-critical column is related to the ability of the splices to continue transferring the maximum developed tensile stress (i.e. once the developable tensile stress starts dropping, lateral failure occurs). Assuming that tensile stress transfer along splices is through a shear-friction mechanism, the stress transfer capability of a splice is expressed in terms of a clamping coefficient which is defined as the ratio of tensile force in the splice to the clamping force from the transverse reinforcement, that is, $A'_s f_s / A_v f_{yt}(l_{s,prov}/s)$ (see Equation 3 and Figure 5A).

$$\theta_p = \lambda_o a_{nl,0} \leq 0.03 \tag{2}$$

where λ_o accounts for the influence of axial load on the rotation capacity of the column and it is equal to 1 for $N/A_g f'_c \leq 0.2$ and 0 for $N/A_g f'_c \geq 0.5$. A linear interpolation is required for $0.2 < N/A_g f'_c < 0.5$. $a_{nl,o}$ relates the plastic rotation capacity to the clamping coefficient and can be estimated as:

$$0.75\% \leq a_{nl,o} = 3.9 - 0.9\frac{A'_s f_s}{A_{vt} f_{yt}\left(\frac{l_{s,prov}}{s}\right)} \leq 3\% \tag{3}$$

where A'_s is the area of tensile reinforcement, f_s is the maximum allowable tensile stress in the longitudinal reinforcement (computed as in Elwood et al.[36]), A_{vt} is the transverse reinforcement area, f_{yt} is the yield strength of the stirrups, s is the stirrup spacing, and $l_{s,prov}$ is the provided splice length. Equation (2) provides a plastic rotation capacity estimate with a mean ratio of observed to calculated of 1.05 and CoV of 11.4% (See Figure 5B).

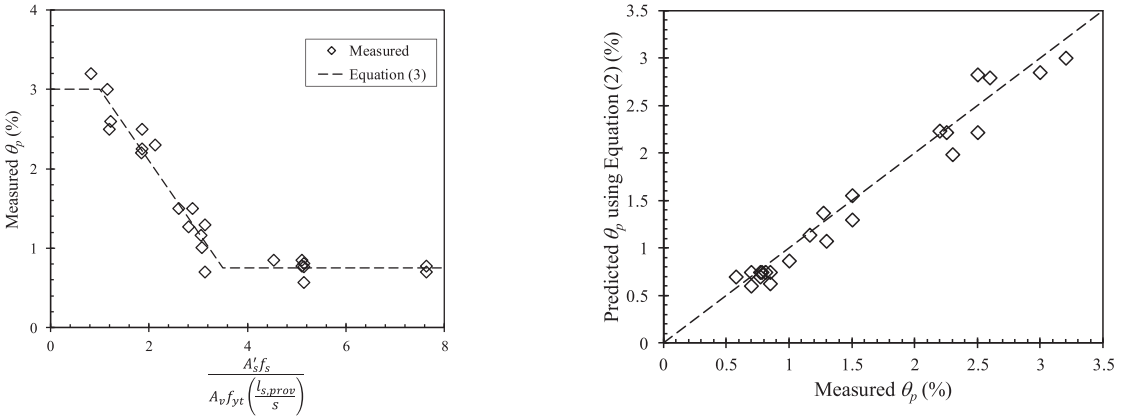

(A) Clamping coefficient vs measured θ_p (B) Measured θ_p vs predicted θ_p using Equation (2)

FIGURE 5 Adequacy of formulation for predicting pre-capping rotation capacity (θ_p) (data available in Opabola and Elwood[17]). (A) Clamping coefficient versus measured θ_p and (B) measured θ_p versus predicted θ_p using Equation (2)

Post-capping rotation capacity (θ_{pc})

The rocking model (Equation 4) proposed by Opabola et al.[37] for evaluating the plastic rotation capacity at the axial failure of columns with smooth reinforcement is adopted here for predicting the plastic rotation capacity at axial failure (b_{nl}) of bond-critical columns with short splices. The adoption of the rocking model is in line with experimental evidences[10,11] that the response of bond-critical columns, following splice failure, is similar to that of a rocking body.

$$b_{nl} = 0.2K\frac{h}{a}\left[1 - \frac{N}{0.7f'_c A_g}\right] \tag{4}$$

where h is the column depth, a is the shear span the coefficient K accounts for the effect of aspect ratio on the rocking behaviour of RC columns:

$$K = 0.5\left(\frac{a}{d}\right) - 0.4 \tag{5}$$

In this study, without loss in accuracy, we further simplify Equation 5 into 6 by assuming that the column effective depth is equal to 80% of the column depth.

$$K = 0.5\left(\frac{a}{d}\right) - 0.4 \approx 0.4\left(\frac{a}{d}\right) = 0.4\left(\frac{a}{0.8h}\right) = 0.5\left(\frac{a}{h}\right) \tag{6}$$

We also further assume that concrete damage due to vertical bond-splitting cracks reduces the undamaged column depth to the depth of the concrete core (assumed to be 0.6 h); such that A_g is replaced with A_c (assumed to be $0.6A_g$) in Equation (4).

Replacing A_g with A_c (assumed to be $0.6A_g$) and replacing K with Equation (6), Equation (4) is simplified into Equation (7).

$$b_{nl} = 0.2K\frac{h}{a}\left[1 - \frac{N}{0.7f'_c A_g}\right] = 0.1\left[1 - \frac{N}{0.42f'_c A_g}\right] = 0.1 - 0.25\frac{N}{f'_c A_g} \tag{7}$$

The adequacy of Equation (7) is shown in Figure 6. Equation (7) provides an estimate with a mean measured-to-calculated ratio of 1.1 and a CoV of 14.5%. Due to limited data, to avoid overestimating the plastic rotation capacity at the axial failure of bond-critical columns, it is recommended that in adopting Equation (7) $N/A_g f'_c$ should not be taken less than 0.1.

The post-capping rotation capacity (θ_{pc}) of a bond-critical column with a short splice can be estimated as the difference between b_{nl}, computed from Equation (7), and pre-capping rotation capacity (θ_p) as computed using Equation (2).

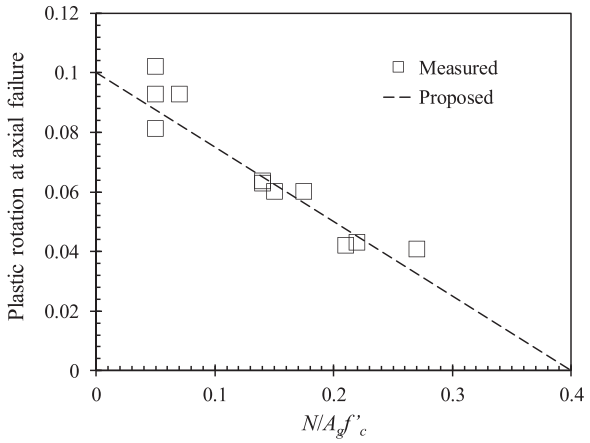

FIGURE 6 Adequacy of Equation (7)

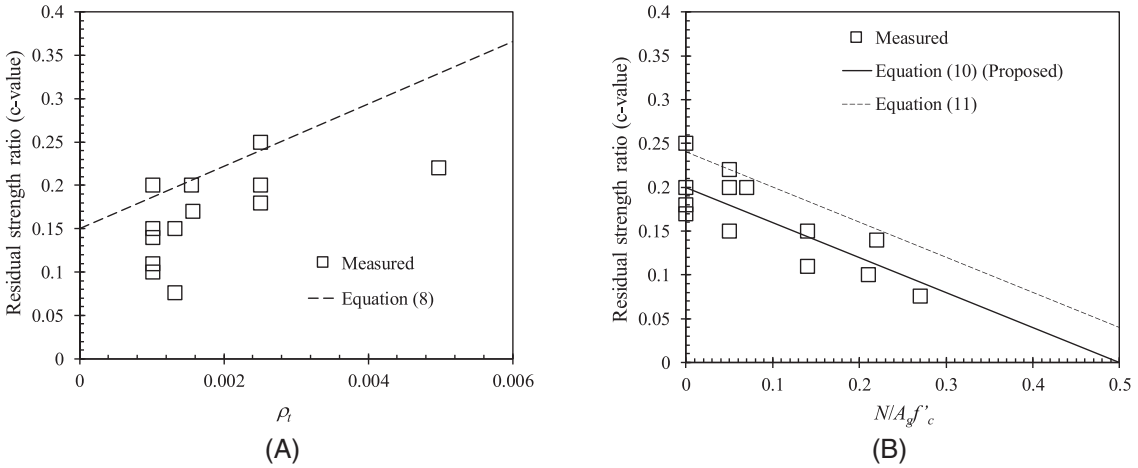

FIGURE 7 Relationship between residual strength ratio and (A) transverse reinforcement ratio and (B) axial load ratio

Residual strength ratio (M_{res}/M_b)

The residual strength ratio, defined as the ratio of residual resistance (M_{res}) to the strength corresponding to the maximum developable tensile stress (M_b), of the bond-critical column dataset in the Opabola and Elwood[17] study, was measured. ASCE/SEI 41-17 adopts Equation (8), as a function of transverse reinforcement ratio (ρ_t), for predicting the residual strength ratio c of bond-critical columns. The adequacy of Equation (8), as well as a proposed recommendation, is presented in this section.

$$c = 0.15 + 36\rho_t \leq 0.4 \tag{8}$$

Figure 7A shows that Equation (8) overestimates the residual strength ratio of bond-critical columns with a mean measured-to-calculated ratio of 0.77 and CoV of 26%. Hence, it was decided to develop a refined formulation to predict the residual strength ratio of bond-critical columns.

The statistical relationship between the measured residual strength ratio, axial load ratio and transverse reinforcement ratio is presented in Table 1. While Figure 7A suggests that the residual strength ratio is well-correlated with the transverse reinforcement ratio (i.e., the governing parameter, according to ASCE/SEI 41-17), Figure 7B and Table 1 suggest that axial load ratio is more correlated with residual strength ratio (correlation coefficient of 0.82). Table 1 also suggests that the correlation between residual strength ratio and transverse reinforcement ratio (correlation coefficient of 0.6) may be largely attributed to the correlation between axial load ratio and transverse reinforcement ratio (correlation coefficient of 0.48).

TABLE 1 Correlation coefficients between measured residual strength ratio (c), transverse reinforcement ratio (ρ_t) and axial load ratio ($N/A_g f'_c$)

	ρ_t	$N/A_g f'_c$	c
ρ_t	1		
$N/A_g f'_c$	−0.48	1	
c	0.60	−0.82	1

TABLE 2 Adequacy of formulations

		Measured/computed			
Model	***R2***	**Minimum**	**Maximum**	**Mean**	**CoV(%)**
Equation (8)	−0.74	0.38	1.07	0.8	25.5
Equation (9)	0.73	0.8	1.34	1.0	17
Equation (10) (proposed)	0.68	0.8	1.25	1.0	17.7
Equation (11)	0.06	0.57	1.04	0.8	19

Linear regression analyses were carried out to develop a formulation for predicting the residual strength ratio of bond-critical columns. Two equations were developed for predicting the residual strength ratio of bond-critical columns – the first considering axial load ratio and transverse reinforcement ratio (Equation (9)) and the second considering axial load ratio only (Equation (10)).

$$c = 0.18 + 12\rho_t - 0.4\frac{N}{A_g f'_c} \geq 0.0 \tag{9}$$

$$c = 0.2 - 0.4\frac{N}{A_g f'_c} \geq 0.0 \tag{10}$$

Equation (10) looks similar to the ASCE/SEI formulation for predicting the residual strength ratio provision for columns not controlled by inadequate development or splicing along with the clear height (See Equation (11)). As shown in Figure 7B, however, Equation (11) overestimates the residual strength ratio of bond-critical columns.

$$c = 0.24 - 0.4\frac{N}{A_g f'_c} \geq 0.0 \tag{11}$$

The adequacy of Equations (8–11) is presented in Table 2. As shown in Table 2, Equation (8) has the least accuracy. The inclusion of transverse reinforcement ratio does not make Equation (9) superior to Equation (10) (See Table 2); hence, Equation (10) is proposed for predicting the residual strength ratio of bond-critical columns. A comparison of Equation (10) with the measured residual strength ratio of bond-critical columns is presented in Figure 7B.

Cyclic strength and stiffness deterioration parameter (Λ) and pinching behaviour parameter (κ)

The hysteretic energy dissipation-based cyclic deterioration rules incorporated in the IMK were developed by Rahnama and Krawinkler.[38] As defined in Rahnama and Krawinkler, the cyclic deterioration in excursion i is defined by the parameter β_i and expressed as:

$$\beta_i = \left(\frac{E_i}{E_t - \sum_{j=1}^{i} E_j}\right)^c \tag{12}$$

where E_i is the hysteretic energy dissipated in excursion i, E_t is the hysteretic energy dissipation capacity and $E_t = \lambda M_y \theta_p = \Lambda \theta_p$, $\sum E_j$ is the hysteretic energy dissipated in all previous excursions and c is an exponent defining the rate of deterioration (typically taken as 1.0[33]).

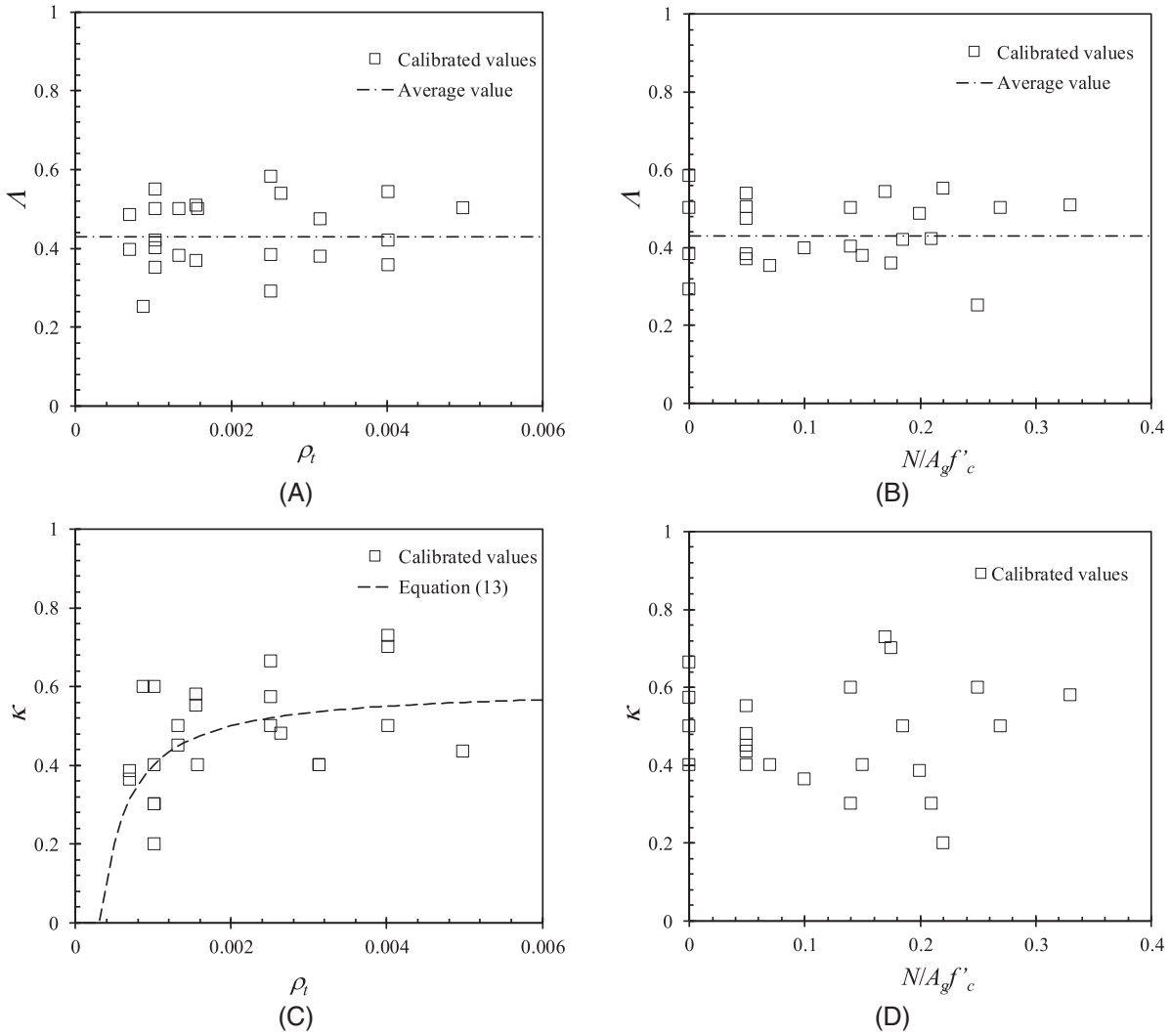

FIGURE 8 The influence of transverse reinforcement ratio and axial load ratio on the calibrated (A and B) Λ and (C and D) κ

The parameter β can be used to incorporate various types of strength and stiffness deterioration phenomena into the hysteresis model. Using a procedure similar to that adopted in previous studies,[33,39] the hysteretic and pinching parameters (Λ and κ) were calibrated to the hysteretic force-displacement response for 24 bond-critical columns in the database compiled by Opabola and Elwood.[17]

Existing literature[40] have shown that cyclic degradation is highly dependent on the axial load level and confinement of the concrete core. It is known that cyclic energy dissipation capacity reduces as axial load level increases or confinement level reduces. The influence of axial load ratio and transverse reinforcement ratio on the calibrated hysteretic and pinching parameters are shown in Figure 8. As shown in Figure 8A and B, Λ is not significantly influenced by the considered variables. The modest variation in Λ values between test specimens may be attributed to the fact that axial load ratio and transverse reinforcement ratio are implicitly included in E_t through θ_p (See Equations 2 and 12). For the dataset, the mean calibrated value of Λ equals 0.42 with a CoV of 19%. For the purpose of modelling bond-critical columns, a value of 0.4 is recommended for Λ. Given the scarcity of experimental data, additional test data are needed to further validate the recommendations provided here.

The pinching parameter κ is defined in Figure 3B. Figure 8C and D suggest that κ reduces as confinement level reduces. The relationship between κ and transverse reinforcement ratio can be expressed using Equation (13). Equation (13) provides an estimate with a mean measured-to-calculated ratio of 1.03 and CoV of 26%. Given the scarcity of experimental

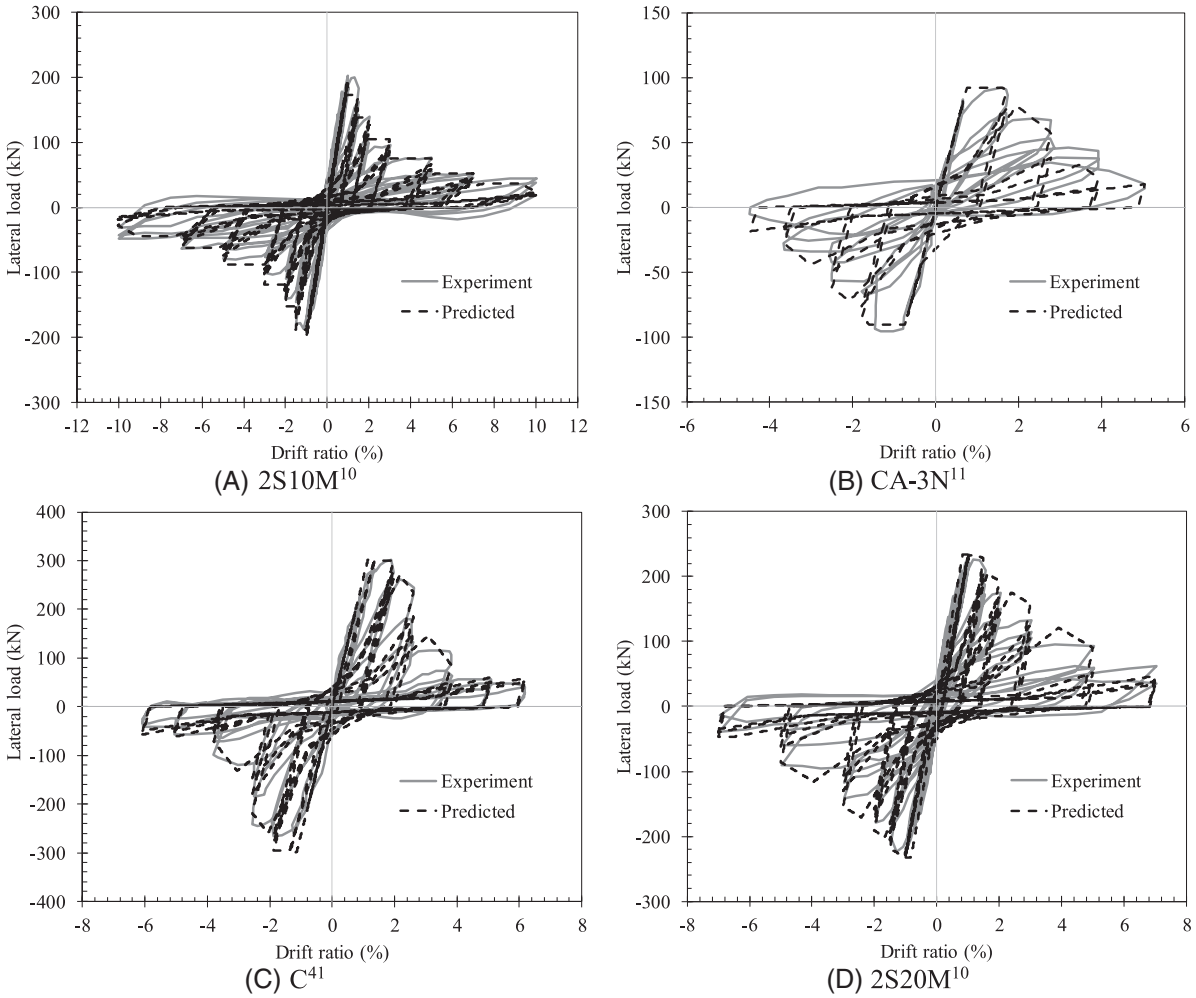

FIGURE 9 Illustration of the adequacy of proposed modelling approach in comparison to cyclic experimental response of bond-critical columns

data, additional test data are needed to further validate the recommendations provided here.

$$\kappa = 0.6 - \frac{0.0002}{\rho_t}, \text{where} \kappa \geq 0 \tag{13}$$

A comparison of numerical and experimental results[10,11,41] from test specimens subjected to cyclic loading protocol is presented in Figure 9. As shown in Figure 9, the force-displacement response of bond-critical columns with short splices are well captured using the proposed approach. The proposed approach is recommended for adoption in ASCE/SEI 41.

3.2.2 | Modelling shear-critical and flexure-shear critical columns with short splices

A number of approaches have been proposed for modelling the response of shear-critical columns. Elwood[42] developed a shear limit-state material that can be combined with fibre elements or flexural rotation spring elements. In the Elwood approach, once the flexural force-displacement curve reaches the shear failure limit surface, a nonlinear shear spring is activated. The activated nonlinear spring controls strength and stiffness deterioration. Axial failure can be detected using the Elwood axial limit-state material. LeBorgne and Ghannoum[43] proposed a pinching limit-state material that works with a force-based and/or deformation-based limit surface, triggering a degrading behaviour when a force and/or deformation limit is reached.

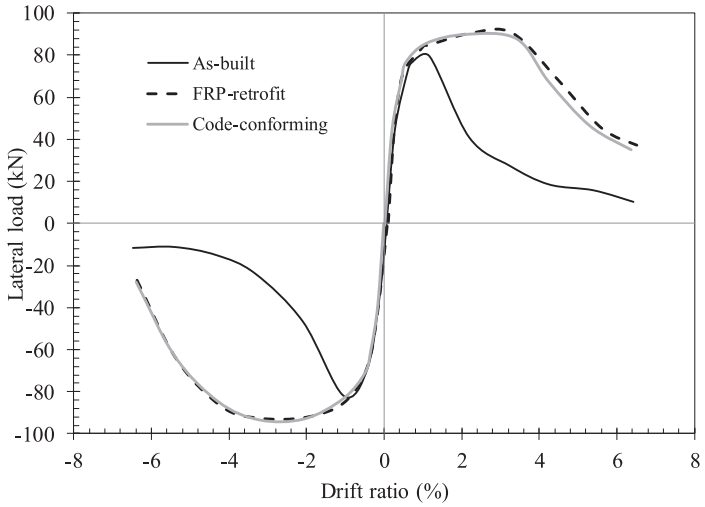

FIGURE 10 Measured backbone curves for an as-built column specimen with lap-splice deficiency, FRP-retrofitted and code-conforming column specimens (data from Harajli and Dagher[12])

Similar to the rotation spring element proposed for bond-critical columns, Haselton et al.[33] have proposed approaches for modelling the cyclic response of flexure and flexure-shear critical columns using zero-length rotational spring elements controlled by trilinear backbone curves.

The three aforementioned approaches can be adopted for modelling flexure-shear critical and shear-critical columns with short splices. For the purpose of the current study, however, the Elwood[42] approach has been adopted. It is noteworthy that test data from shear-critical and flexure-shear critical columns with short splices were part of the dataset adopted in calibrating the modelling parameters for the Elwood[42] approach.[26,44]

3.3 | Modelling FRP-retrofitted columns with short splices

One significant challenge to evaluating the collapse fragility of retrofitted buildings is the fact that state-of-the-art seismic assessment procedures do not provide guidance on acceptance criteria and modelling parameters for retrofitted columns. Studies[45,46] have modelled retrofitted columns using fibre-element models with the confined concrete backbone properties modified to account for the enhanced confinement from the FRP wrapping or steel jacketing. In the aforementioned studies, 'additional' bond-slip deformation is typically modelled using a rotational bond-slip spring.

A key attribute of fibre-element models is their capability to capture inelastic deformations due to flexural curvature. Experimental results[12,47,48] on jacketed columns with short splices have, however, shown that fixed-end rotation accounts for up to 80% of total deformation during the inelastic phase. In fact, the main difference between as-built bond-critical columns and the retrofitted bond-critical columns is the enhanced deformation capacity and energy dissipation capacity, lesser pinching, lower strength and stiffness deterioration rates as a result of the improved concrete-rebar bond and external confinement to the concrete provided by the jackets. Hence, it may be more appropriate to explore the applicability of a lumped plasticity model to better capture the concentration of inelastic deformation at the column ends.

For the purpose of this study, experimental data from cyclic tests on FRP-retrofitted bond-critical columns with short splices were examined.[11,12,49] In some of the examined test programs, a code-conforming column specimen had also been tested in order to compare the retrofit effectiveness. Figure 10 compares the measured force-displacement backbone response of an as-built bond-critical critical with short splices with those of an FRP-retrofitted nominally identical column, and a code-conforming column (i.e., continuous longitudinal reinforcement and conforming stirrup detailing). As shown in Figure 10, the response of the FRP-retrofitted column specimen was nearly identical to that of a code-conforming column, with very similar flexural strength and deformation capacity. The authors[12] also noted that the energy absorption capacity of the FRP-retrofitted and code-conforming column specimens were similar.

In this study, it is recommended that the behaviour of the FRP-retrofitted column can be modelled using a hinge model (Figure 3). The recommended modelling parameters FRP-retrofitted columns are described below.

As reported in previous studies,[50,51] effective stiffness formulations developed for regular columns are generally applicable to FRP-retrofitted columns. Hence, Equation (1) is also adopted for FRP-retrofitted columns.

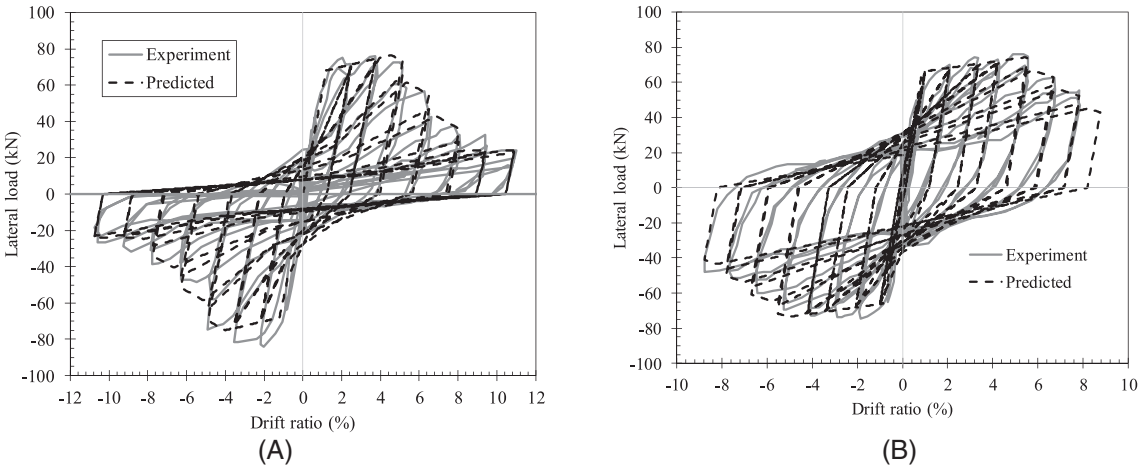

FIGURE 11 Illustration of adequacy of a proposed modelling approach for retrofitted columns in comparison to cyclic experimental response (test data from Ghosh and Sheikh[11])

As earlier mentioned, the spread of plasticity in FRP-retrofitted columns with short splices is mainly through strain penetration. The equivalent plastic length (L_p)[51] of an FRP-retrofitted column can be evaluated as $g + 0.044 f_y\, d_b$; where g is the gap between the jacket and the footing, $0.044 f_y\, d_b$ is the strain penetration length, f_y and d_b are the yield strength and diameter of the longitudinal reinforcement respectively. The pre-capping rotation capacity of the FRP-retrofitted column $\theta_p = (\phi_u - \phi_y)L_p$,[51] where ϕ_u and ϕ_y are the ultimate and yield curvatures of the column and are estimated through a moment-curvature analysis. In this study, however, we recognise that in certain cases (e.g. under low axial load), FRP-retrofitted columns may suffer bar fracture rather than concrete compression failure;[50] hence the ultimate curvature capacity is defined to correspond to a tensile strain of 0.06[52] or a concrete compressive strain accounting for the FRP-enhanced confinement level.[51] It is also noteworthy that the column yield strength (M_y) and peak strength (M_{max}) for defining the moment-rotation relationship of the retrofitted column are outputs of the moment-curvature analysis.

As described in experimental studies[12] and shown in Figure 10, the post-capping response of FRP-retrofitted and modern columns are similar. For lack of appropriate formulations specifically calibrated to a large database of FRP-retrofitted columns, it is recommended that the post-capping plastic rotation capacity (θ_{pc}) of an FRP-retrofitted column be computed using formulations proposed by Haselton et al.[33] using equivalent transverse reinforcement (stirrups) parameters and the axial load level, force-displacement nonlinear modelling parameters. The definition of the equivalent reinforcement parameters is defined as follows:

The confinement level provided by the FRP wrapping can be expressed in terms of an equivalent volumetric transverse reinforcement ratio ($\rho_{v,eff}$):

$$\rho_{v,eff} = \rho_f \left(\frac{f_f}{f_{yt}} \right) \tag{14}$$

where f_f is the strength of the FRP wrapping in the hoop direction, f_{yt} is the yield strength of the transverse reinforcement in the column, and ρ_f is the FRP volumetric reinforcement ratio, computed in accordance with ACI 440.[53]

Similar to the procedure previously adopted by Alvarez and Brena,[54] assuming an area of transverse reinforcement $A_{v,eff}$, the equivalent transverse reinforcement s_{eff} corresponding to the equivalent volumetric transverse reinforcement ratio (evaluated using Equation (14)) can be computed, such that the provided FRP wrapping can be expressed as equivalent stirrups with yield strength of f_{yt}, area of $A_{v,eff}$ and spacing of s_{eff}.

Figure 11 shows the adequacy of the proposed modelling approach for FRP-wrapped bond-critical columns tested by Ghosh and Sheikh.[11] As shown in Figure 11, the cyclic response of the test specimens is well captured using the proposed approach. Additional studies are needed to explore the applicability of this approach to other jacketed beam-column components with continuous deformed bars as well as with continuous and spliced plain bars.

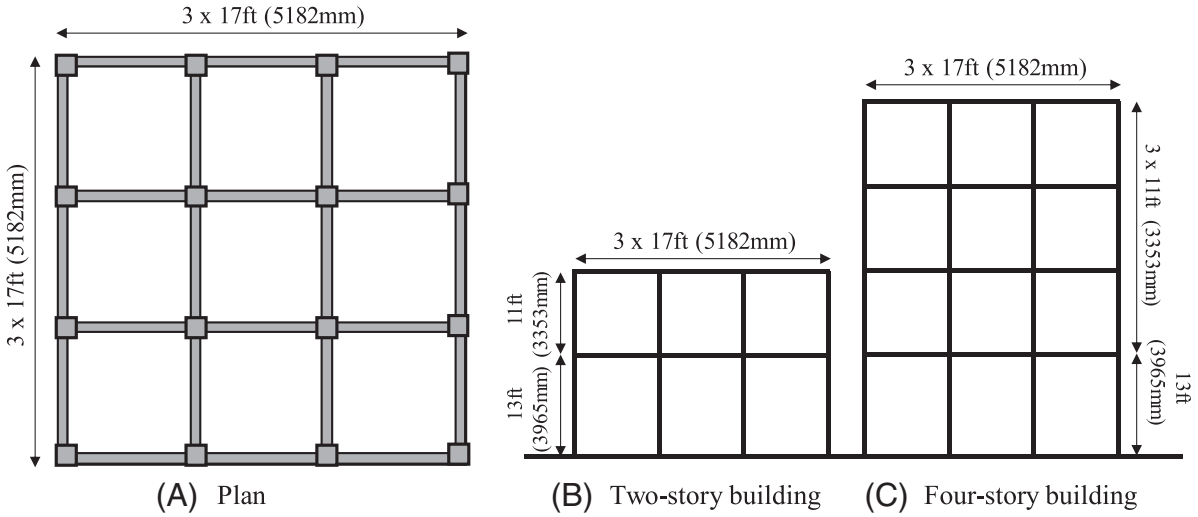

FIGURE 12 Case-study buildings. (A) Plan, (B) two-story building and (C) four-story building

4 | CASE STUDY BUILDINGS

4.1 | As-built concrete frames

For the purpose of this study, a set of two-story and four-story space frame structures, designed according to the 1967 Uniform Building Code,[18] were considered. Each of the archetype frame structures is assumed to be situated at a Southern California site with coordinates 33.996°N, –118.162°W. Inventory studies[55] have shown that about 70% of pre-1980s RC structures in high seismic regions of the United States are between 1 and four stories. It is also noteworthy that the archetype frame structures, adopted in this study, are also representative of pre-1980s RC frame buildings in other seismically active regions, for example, New Zealand. A survey of RC frames constructed in Wellington, New Zealand between 1935 and 1975 showed that 52% of buildings were 2–3 stories and about 21% are 4–6 stories.[56]

The archetype frame structures consist of three bays of equal widths (17 ft (5182 mm)), a ground story height of 13 ft (3965 mm) (see Figure 12). A constant story height of 11 ft (3353 mm) was adopted for the remaining stories in the building. As expected in structures from the design era, it was assumed that the floor slabs with a thickness of 8 in (~200 mm) were monolithically cast with the beams. The expected combinations of dead load (DL) and live load (LL) under seismic demands,[57] on the structure (comprising dead load and live load) was taken to be equal to 209 psf (10 kPa).

All the structural components were designed using the working stress design method, as was typical of the era. For each structure, the column dimension (18 in by 18 in (457 mm x 457 mm)) and reinforcement detailing (longitudinal reinforcement ratio of 1.9% and transverse reinforcement ratio of 0.26%) were kept constant over the height of the building. Each beam is 30 in (762 mm) deep and 18 in (457 mm) wide. It is assumed that the splices in the beams are not located in their plastic hinge regions. Typical of pre-1970s structures, the beam-column joints were unreinforced.

After the design, the column and beam strengths were compared. For the internal and external subassemblies, the values of $\Sigma Mc/\Sigma Mb$ correspond to 0.47 and 0.77, confirming that a column mechanism was the most probable mechanism. Also, the equivalent column moment corresponding to joint shear failure computed following the strength hierarchy approach,[58] was higher than the column yield strength – making joint failures unlikely. It is noteworthy that a number of experimental studies[59] have tested as-built and retrofitted RC soft-storey frame structures with splice-deficient columns, similar to case-study buildings in this paper.

For each building type, three variations were considered, making a total of six buildings. The first variation assumes that the columns have straight splices with a splice length corresponding to $30d_b$ in the plastic hinge region of all columns in the building. Using the failure mode identification approach,[17] these columns are predicted to be bond-critical.

The second variation assumes the splice lengths in the columns were increased to $35d_b$, which is sufficient for the longitudinal reinforcement to reach its yield strength, and the columns able to attain their flexural yield capacity. As a

result of the shear capacity ratio of the columns ($V_p/V_n \approx 0.8$), however, they are susceptible to a flexure-shear critical mechanism as observed in tests.[25,30]

Finally, for the third variation, the columns of the first variation were retrofitted to avoid a splice or shear failure. The design of this retrofit is described below.

4.2 | Seismic evaluation and retrofit design in accordance with ASCE/SEI 41-17

In this study, retrofits of the splice-deficient columns are designed according to ASCE/SEI 41-17 Tier 3. Prior to retrofit design, the behaviour of each as-built frame was evaluated using the nonlinear dynamic procedure (NDP) in accordance with section 7.4.4 of ASCE/SEI 41-17. The adopted hinge-type models are as described previously in this paper. Nonlinear response history analyses were carried out to evaluate the structural performance of each as-built structure at BSE-2E hazard level (computed as $S_{X1} = 0.87$ g; $S_{XS} = 1.38$ g). The site-specific seismic hazard was characterised based on the US Geological Survey (USGS) hazard maps. The structures are classified as Risk Category II and a site class D soil was assumed. For the two- and four-story structures, 11 ground motion records were selected using the conditional mean spectrum approach.[60]

While according to ASCE/SEI 41-17, the building performance level is defined as the combination of the performance levels of nonstructural and structural systems, in the current study, however, only the structural performance levels are considered. Under the BSE-2E hazard level, a structure must fulfil the CP structural performance level. Analytical results showed that the as-built structures do not fulfil the CP structural performance level at the BSE-2E hazard level. Further discussions on the seismic fragility of the as-built structures at various performance objectives are presented subsequently in this paper. Here, we design the retrofit to achieve CP structural performance level at the BSE-2E hazard level for comparison with the as-built buildings.

The choice of retrofit technique is heavily influenced by economic considerations, desired continued functionality of the building during the retrofit, and desired global inelastic mechanism for the retrofitted structure. Retrofit strategies can be in form of component-level and subassembly-level modifications (e.g., selective strengthening using jacketing techniques or selective weakening techniques) and/or system-level modifications (including, but not limited to, structural strengthening, structural stiffening, mass reduction, or removal of potential structural weaknesses).

Three retrofit techniques were considered – concrete jacketing, steel jacketing and FRP wrapping. However, the FRP-wrapped column was preferred as the column dimension remains almost the same, thereby keeping the useable floor area unchanged. Also, desirably, the natural period of the structure is unchanged. In addition, previous studies have shown that well-designed FRP-wrapped and steel-jacketed columns are able to achieve similar improvement in deformation capacities,[61] so results may be similar in both cases.

The ASCE/SEI 41-17 Tier 3 evaluation was adopted for the retrofit design. The retrofit was intended to improve the drift capacity and energy dissipation capacity of the columns. The FRP retrofit design entailed providing confinement to ensure sufficient clamping is provided to inhibit splice failure and also improve the shear strength of the columns. The FRP retrofit design was carried out in accordance with ACI 440[53] provisions. A shear capacity ratio of 0.6 is desirable to achieve a flexure-dominated mechanism. For the purpose of this study, however, a V_p/V_n of 0.4 was targeted as this value corresponds to the shear capacity ratio of a modern column with similar cross-section and transverse reinforcement conforming to ACI 318–19.[23]

5 | NONLINEAR SIMULATION MODELS OF ARCHETYPE STRUCTURES

The two archetype buildings described in the previous section are symmetric in the plan; hence, it is assumed that the structures respond to ground motion excitation without any torsional behaviour. Each of the six aforementioned variations was modelled using a two-dimensional frame that corresponds to one of the interior frames of the structure. The seismic mass of the frame was lumped at each beam-column joint and the ground floor columns were assumed to be fixed at the foundations and the floor diaphragms were assumed rigid. The beams were modelled using a combination of elastic beam-column elements and zero-length nonlinear rotational spring elements following the Haselton et al.[33] approach. The columns were modelled using the approaches described previously in Section 3. As noted previously, a joint mechanism was not expected to govern the behaviour, and, hence, no explicit joint modelling was incorporated in

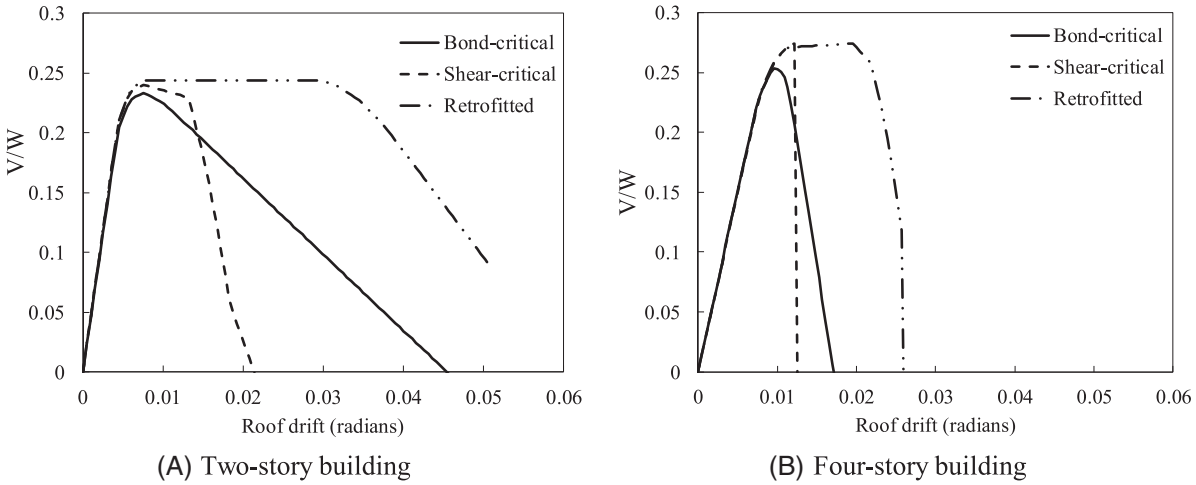

FIGURE 13 Pushover curves for the considered buildings with different column characteristics. (A) Two-story building and (B) four-story building

the building models. To capture the additional flexibility from the joints, following ASCE/SEI 41-17 provisions, the joints were modelled implicitly by assuming rigid offsets in the beams only (for $\Sigma M_c/\Sigma M_b < 0.8$).

To account for nonlinear geometric effects, the P-delta transformation incorporated in OpenSees was employed. Damping was modelled using a value of 2% for Rayleigh damping in the first and third modes.[9,14,62] The fundamental period from eigenvalue analysis with the effective stiffness assumptions described above of the two-story building model is 0.71 s. The fundamental period of the four-story building model is 1.24 s.

6 | NONLINEAR ANALYSES

6.1 | Pushover analyses

Nonlinear pushover analyses, using inverted triangular load pattern was performed on each of the six building variations – two- and four-story buildings with bond-critical, flexure-shear critical (hereafter referred to as shear-critical for brevity) and retrofitted columns. Figure 13 plots the base shear versus roof drift relationship for all six variations. The base shear has been normalised by the seismic weight on the frame. As shown in Figure 13, the retrofitted structure has the highest deformation capacity. The buildings with shear-critical columns had a sharp drop in strength which is attributed to significant degradation in lateral resistance after lateral failure in the ground floor columns. In comparison, despite experiencing the earliest onset of lateral resistance degradation, the buildings with bond-critical columns were able to resist a significant amount of lateral shear demands at large drift ratios.

6.2 | Incremental dynamic analysis

The collapse behaviour of each building variation was assessed using the incremental dynamic analysis (IDA) approach.[63] A suite of 22 pairs of recorded far-field ground motions representative of large seismic events were adopted from FEMA P-695.[64] The magnitude and distance for the ground motion records in the adopted suite were larger than $M_w = 6.5$ and 10 km, respectively.

For each model, the maximum story drift demand and spectral acceleration corresponding to the fundamental period ($S_a(T_1)$) were recorded. Global collapse capacity was defined to correspond to the smallest scaling of a ground motion sufficient to achieve either a maximum inter-story drift of 10% or when θ_{pc} (see Figure 3B) of 50% of the columns at any story level is exceeded. This approach has previously been adopted by Galanis and Moehle.[14]

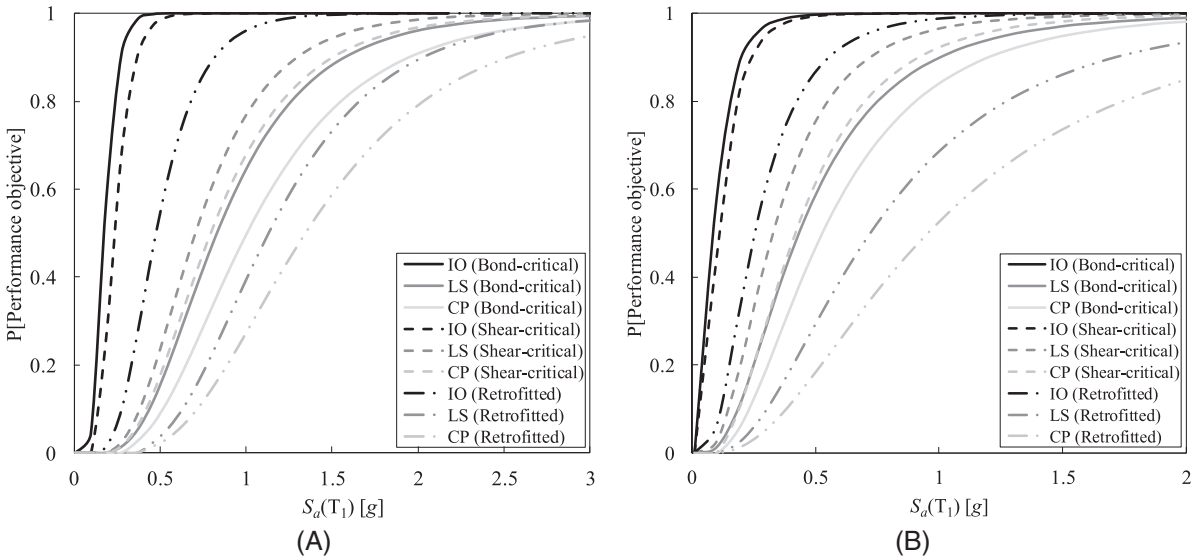

FIGURE 14 IO, LS and CP fragility curves for (A) two-story building and (B) four-story building, respectively

7 | GLOBAL SEISMIC ASSESSMENT OF BUILDINGS

7.1 | Seismic fragilities at different performance objectives

Using results from the IDA analyses, the responses of all structures were analysed for four different limit states. The first three limit states are based on the ASCE/SEI 41-17 performance objectives, while the last limit state corresponds to the collapse capacity as defined in the previous section. ASCE/SEI 41-17 makes provisions for seismic assessment to satisfy three performance objectives – IO, LS and CP. For the sake of brevity, these performance objectives are not defined here and interested readers are referred to ASCE/SEI 41-17. The acceptance criteria for different RC components to satisfy each of the aforementioned ASCE/SEI 41-17 performance objectives, as fractions of inelastic rotation capacities at lateral (a) and axial failure (b), are provided in Chapter 10 of the standard. For reinforced concrete columns, the IO limit is defined to correspond to an inelastic rotation capacity of zero for bond-critical columns and $0.15a \leq 0.5\%$ for other failure modes. LS and CP performance objective limits correspond to $0.5b$ and $0.7b$, respectively (See Table 10–8 of ASCE/SEI 41-17). For bond-critical columns, the corresponding drift ratios to these limits were computed using Equations (2) and (4).

Fragility functions for each limit state were developed using results from IDA on the six buildings. Assuming a lognormal distribution for the demand and capacity, the probability of reaching or exceeding a specified damage state given an intensity measure (IM) can be estimated as:

$$P\left[D > C \,|\mathrm{IM}\right] = \Phi\left[\frac{\mathrm{In}\left(S_D/S_C\right)}{\sqrt{\beta_{D|IM}^2 + \beta_C^2 + \beta_M^2}}\right], \tag{15}$$

where D and C are the seismic demand and structural capacity, respectively; S_D and S_C are the median values of the demand and structural limit state, respectively; $\beta_{\mathrm{D|IM}}$ is the record-to-record uncertainty as a function of $\mathrm{S_a(T_1)}$; β_C is the dispersion of all limit states and is taken as 0.3[65]; and β_M is the modelling uncertainty and is taken as 0.2.[66]

The obtained fragility curves for the IO, LS and CP performance objectives for the two- and four-story buildings are presented in Figure 14. The collapse fragilities for the buildings are presented in Figure 15. As shown in Figure 14, the structures with the bond-critical columns have the lowest median $S_a(T_1)$ for the IO performance level. This is not surprising given that the IO drift limit for the bond-critical column corresponds to an inelastic rotation that equals zero. The buildings with bond-critical columns, however, have larger $S_a(T_1)$ values at the LS and CP limit states than the shear-critical buildings. This superior performance is attributed to the fact that both limit states are a function of inelastic rotation capacity at axial failure and the rocking mechanism in bond-critical columns is sufficient to delay axial failure following splice failure. For the LS, CP, and collapse limit states, the median $S_a(T_1)$ values for the bond-critical buildings are about

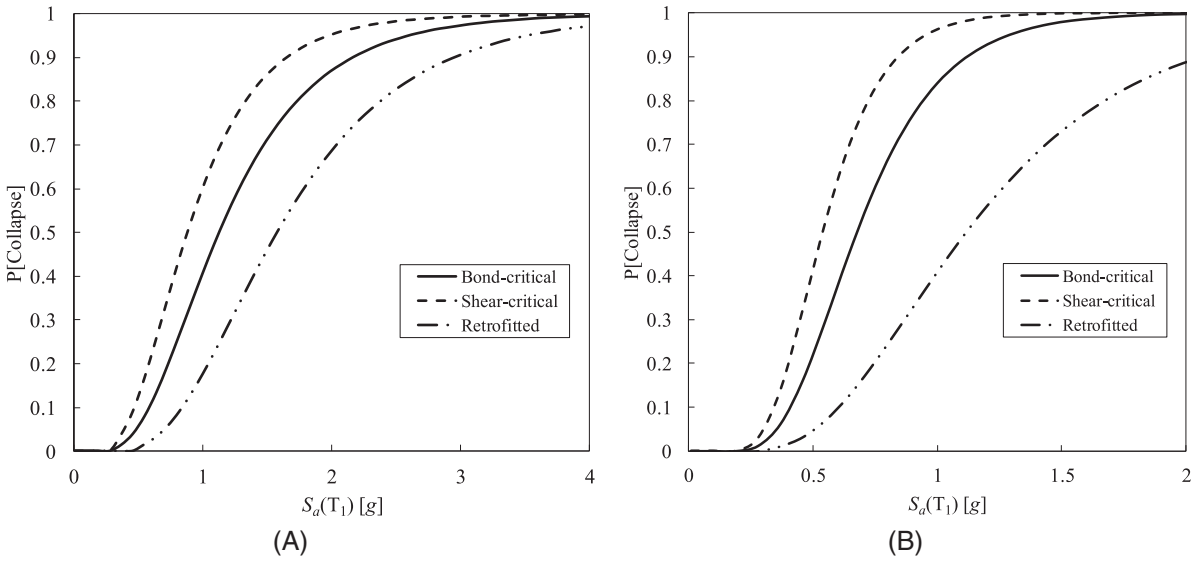

FIGURE 15 Collapse fragility curves for (A) two-story building and (B) four-story building

30% larger than that of the shear-critical buildings. It is worth recalling that the only difference between the bond-critical and shear-critical columns was a splice length of $30d_b$ for bond-critical versus $35d_b$ for shear-critical; hence, a shorter splice length is in fact resulting in an improved LS, CP, and collapse performance.

Regardless of the number of stories, the retrofitted buildings have the largest median $S_a(T_1)$ values at all limit states. At the collapse limit state, the median $S_a(T_1)$ values of the two- and four-story retrofitted buildings are 80 and 120% larger than the two- and four-story buildings with shear-critical columns. Likewise, the median $S_a(T_1)$ values of the two- and four-story retrofitted buildings are 36 and 70% larger than the two- and four-story buildings with bond-critical columns.

It is noted, however, that the two- and four-story case study buildings do not include columns with high axial loads (i.e. axial load ratio greater than 35%). At high axial loads, bond-critical columns with light transverse reinforcement may fail at similar drifts to that of shear-critical columns. A higher level of axial load may also trigger flexure-shear interaction. The likelihood of this interaction needs to be assessed on a case-by-case basis as it is also dependent on the geometric, material and reinforcement detailing. Also, the results presented in this study may not be valid for buildings dominated by a joint mechanism.

7.2 | Influence of reinforcement detailing on collapse performance

As previously discussed, columns in older type buildings typically have light transverse reinforcement with lap-spliced or continuous longitudinal reinforcement. The probable failure mode of these columns is dependent on this reinforcement detailing. Figure 16 presents the influence of longitudinal reinforcement detailing on the median collapse fragility of the original two- (2S-U) and four-story (4S-U) buildings with varying splice length in the columns. As shown in Figure 16, due to inadequate transverse reinforcement detailing, the seismic performance of buildings with provided splice length sufficient to attain flexural yield (prior to shear failure) perform worse than the bond-critical columns (i.e., $l_{s,prov} \leq 30d_b$). The axial capacity of shear-damaged columns is not significantly influenced by longitudinal reinforcement detailing (i.e. presence or absence of lap splices).[17,26] Hence, the median collapse fragility of all the buildings with shear-damaged columns (i.e. $l_{s,prov} \geq 35d_b$) is similar. As shown in Figure 16, older type buildings with bond-critical columns may perform better than buildings with shear-critical columns having continuous reinforcement (and sparsely spaced transverse reinforcement) when the response is dominated by a soft-story mechanism.

As shown in Figure 16, for the two- (2S-R) and four-story (4S-R) buildings with retrofitted columns, the provision of additional lateral confinement (from the FRP wraps) in the poorly detailed columns prevents lap-splice and shear failure modes, allowing the column response to be flexure-dominated. For the retrofitted buildings, a similar median collapse fragility was attained (See Figure 16). Figure 16 shows that providing additional lateral confinement in the columns

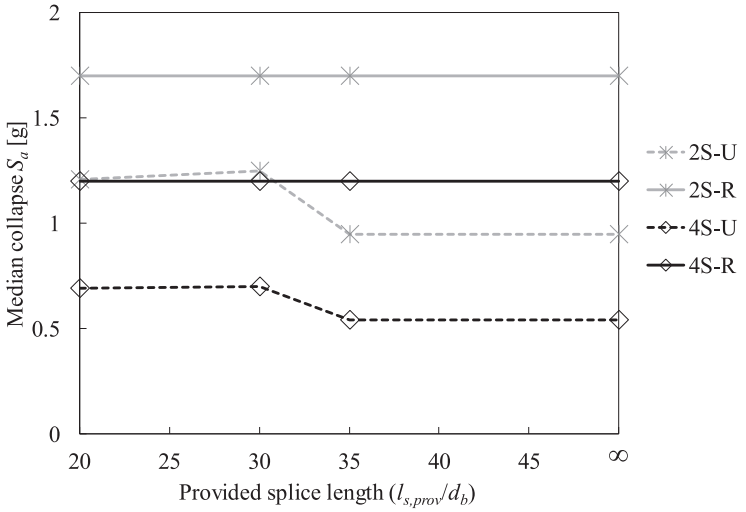

FIGURE 16 Influence of reinforcement detailing of columns on median collapse fragility of the two- (2S) and four-story (4S) frame structures (∞ represents continuous longitudinal reinforcement; U: as-built; R: retrofitted)

TABLE 3 FEMA P-2018 Building rating (BR)

Building model		BR (FEMA P-2018)	BR (proposed)	P(Collapse |BSE-2E)IDA
Two-story	Shear-critical	0.90 (EHR)	0.90 (EHR)	0.75
	Bond-critical	0.90 (EHR)	0.50 (HR)	0.54
	Retrofitted	0.30 (LR)	0.30 (LR)	0.32
Four-story	Shear-critical	0.80 (EHR)	0.80 (EHR)	0.62
	Bond-critical	0.80 (EHR)	0.35 (HR)	0.38
	Retrofitted	0.10 (LR)	0.10 (LR)	0.10

Abbreviations: EHR, exceptionally high risk; HR, high risk; LR, lower risk (according to FEMA P-2018).

switches the relationship between the median collapse S_a and provided splice length from a step function to a linear function.

7.3 | Evaluation of collapse potential using FEMA P-2018 methodology

FEMA P-2018[9] provides a simple methodology for evaluating the collapse potential of older type concrete buildings. This methodology first identifies the critical stories and components for various structural configurations. Then, given a target displacement demand, the collapse potential of a structure can be evaluated based on comparison of drift demands and drift capacities of critical components, as described in the FEMA P-2018 document. The component drift capacities adopted in the methodology are intended to represent the drift at which loss of gravity load-carrying capacity occurs.

Following the FEMA P-2018 methodology, the collapse potentials of the four as-built and the two retrofitted case-study structures were evaluated for a seismic hazard level corresponding to ASCE/SEI 41-17's BSE-2E (i.e., 5% probability of exceedance in 50 years). According to FEMA P-2018, the deformation capacity of columns with short splices can be assessed by assuming the longitudinal reinforcement is continuous and based on the column's shear capacity ratio (V_p/V_n), the failure mode may be categorised as flexure-critical, flexure-shear critical or brittle shear-critical – the bond-critical mechanism is not recognised in terms of its effect on drift demands or drift capacities.

The rating of each building, determined following the FEMA P-2018 methodology, is presented in Table 3. As shown in Table 3, the current FEMA P-2018 approach would assign the same Building Ratings (which is akin to a collapse probability, and higher values indicate greater collapse potential) for the buildings with shear-critical and bond-critical columns. This is because FEMA P-2018 does not currently recognise the higher drift at axial capacity associated with bond-critical columns. However, results from the fragility functions derived from the IDA here show that the buildings have different

collapse probability at the selected hazard level (see Table 3). This discrepancy results in a different relative ranking and assessment of the bond-critical buildings than suggested by the collapse fragility analysis.

We proposed a modified approach for FEMA P-2018 for evaluating the collapse drift capacity of bond-critical columns. If Equation (3) is adopted in computing the plastic rotation capacity at axial failure for bond-critical columns, the influence of the column failure mode on the Building Rating becomes more consistent with the evaluated collapse risk. Considering this proposed modification in assessing the Building Rating (see Table 3), it is evident that buildings with shear-critical columns are more collapse-prone than buildings with bond-critical columns and should be prioritised for retrofit. The buildings with bond-critical columns are, however, still categorised as "High Risk" and, hence, should not be overlooked when developing risk mitigation policies.

8 | CONCLUSIONS

In this study, the seismic performance of as-built and retrofitted pre-1970s RC frame structures with splice-deficient columns was evaluated using probabilistic nonlinear dynamic analysis procedures. In comparison with shear-critical columns (with or without short splices), bond-critical columns with splice deficiencies have a larger buffer between lateral and axial failure. For typical arrangements of transverse reinforcement found in older columns, it was identified that a column failure mode can switch from bond-critical to shear-critical by simply increasing the splice length from $30d_b$ to $35d_b$. FRP wrapping of splice-deficient columns, to improve the bond behaviour of the splice region and the shear capacity of the plastic hinge region, was also considered to demonstrate the improved performance of retrofitted buildings.

As a first step, using experimental data from various studies, simple and efficient hinge models are calibrated to simulate the inelastic hysteretic response of as-built and FRP-retrofitted columns with short splices. In the proposed approach for the as-built column, the probable failure mode was assessed using a strength-based procedure. Thereafter, the force-displacement backbone for the column model was developed using mechanistic formulations for predicting the pre-capping and post-capping rotation capacity of the columns considering the probable failure mode. The adequacy of the proposed approach was demonstrated using experimental data. A limitation in this study is the size of the experimental dataset used in validating the proposed approach. Additional test data are needed to further validate the recommendations provided in this study.

Using the proposed modelling approach, the seismic performance of a set of two- and four-story RC frames was evaluated at different limit states. The response of the considered frames is dominated by a soft-story mechanism. Incremental dynamic analyses, using a suite of 22 pairs of far-field ground motions, showed that the median collapse $S_a(T_1)$ for the retrofitted buildings was 40–70% larger than that of the bond-critical buildings and 80–120% larger than that of shear-critical buildings.

Due to the rocking behaviour of bond-critical columns after splice failure, the median $S_a(T_1)$ for the bond-critical buildings was about 30% larger than that of the shear-critical buildings at three limit states – LS, CP and collapse. This better behaviour of the buildings with bond-critical columns is because the columns were able to sustain their axial load-carrying capacity at large drift demands. However, the shear-critical buildings have a median $S_a(T_1)$ at IO about 33% larger than the bond-critical building because bond-critical columns experience the initiation of bond failure at low drift levels. It is noted, however, that the two- and four-story case study buildings do not include columns with high axial loads. At high axial loads, bond-critical columns with light transverse reinforcement may fail at similar drifts to that of shear-critical columns. Also, the results presented in this study may not be valid for buildings dominated by a joint mechanism.

The collapse potential of each considered building was assessed using FEMA P-2018 provisions. Results showed that, contrary to results from nonlinear dynamic analyses, the current FEMA P-2018 procedures produce ratings of buildings with bond-critical and shear-critical columns that indicate similar collapse potential. This is attributed to the fact that FEMA P-2018 does not account for the bond degradation effect on column deformation capacity. It is, therefore, proposed that future editions of FEMA P-2018 should account for the influence of failure mode on collapse capacity of columns with short splices using approaches proposed in this study.

ORCID

Eyitayo A. Opabola https://orcid.org/0000-0002-7598-4812

Abbie B. Liel https://orcid.org/0000-0002-9241-5144

REFERENCES

1. Kam WY, Pampanin S, Elwood K. Seismic performance of reinforced concrete buildings in the 22 February Christchurch (Lyttelton) earthquake. *Bull New Zeal Soc Earthq Eng*. 2011;44(4):239-278.
2. Norton JA, King AB, Bull DK, et al. Northridge earthquake reconnaissance report. *Bull New Zeal Soc Earthq Eng*. 1994;27(4):235-344.
3. Sezen H, Elwood KJ, Whittaker AS, Mosalam KM, Wallace JW, Stanton JF. Structural engineering reconnaissance of the August 17, 1999 earthquake. UCB/PEER-00/09. Kocaeli, Turkey; 2000. https://doi.org/10.13140/RG.2.1.1324.2483.
4. Otani S. RC building damage statistics and SDF response with design seismic forces. *Earthq Spectra*. 1999;15(3):485-501.
5. Bull DK. Earthquakes and the effects on structures: some of the lessons learnt. *Aust J Struct Eng*. 2013;14(2):145-165.
6. ASCE. Seismic evaluation and retrofit of existing buildings: ASCE/SEI 41-17. American Society of Civil Engineers; 2017. https://doi.org/10.1061/9780784414859
7. MBIE, EQC, NZSEE, SESOC, NZGS. Part C5, concrete buildings, technical proposal to revise the engineering assessment guidelines; 2018. http://www.eq-assess.org.nz/wp-content/uploads/2018/11/Technical_Proposal_to_Revise_C5_30112018.pdf. Assessed online 04 Aug 2020.
8. Desmarais F, Chumko A. Wellington Central Library to close indefinitely due to earthquake concerns. 2019. https://www.stuff.co.nz/dominion-post/news/111397052/wellington-city-library-to-close-after-advice-received-from-engineers. Assessed online 04 Aug 2020.
9. FEMA. Seismic evaluation of older concrete frame buildings for collapse potential. In: Applied Technology Council for the Federal Emergency Management Agency. California: VA; 2018.
10. Melek M, Wallace JW. Cyclic behavior of columns with short lap splices. *ACI Struct J*. 2004;101(6):802-811.
11. Ghosh KK, Sheikh SA. Seismic upgrade with carbon fiber-reinforced polymer of columns containing lap-spliced reinforcing bars. *ACI Struct J*. 2007;104(2):227.
12. Harajli MH, Dagher F. Seismic strengthening of bond-critical regions in rectangular reinforced concrete columns using fiber-reinforced polymer wraps. *ACI Struct J*. 2008;105(8):68-77.
13. Liel AB, Haselton CB, Deierlein GG. Seismic collapse safety of reinforced concrete buildings. II: Comparative assessment of nonductile and ductile moment frames. *J Struct Eng*. 2011;137(4):492-502.
14. Galanis PH, Moehle JP. Development of collapse indicators for risk assessment of older-type reinforced concrete buildings. *Earthq Spectra*. 2015;31(4):1991-2006.
15. Ghannoum WM. Updates to modeling parameters and acceptance criteria for non-ductile and splice-deficient concrete columns. In: 16th World Conference on Earthquake Engineering; Santiago: CL; 2017:1-12.
16. CEN. European Standard EN 1998-3:2005. Eurocode 8: Design of structures for earthquake resistance - part 3: assessment and retrofitting of buildings. In: European Committee for Standardization; Brussells: BE; 2005.
17. Opabola EA, Elwood KJ. Seismic assessment of reinforced concrete columns with short lap splices. *Earthq Spectra*. 2021.
18. ICBO. Uniform building code. In: International Conference of Building Officials; Whittier: CA; 1967.
19. ACI. Building code requirements for reinforced concrete (ACI 318–56): adopted as a standard of the American Concrete Institute at its 52nd Annual Convention, February 21, 1956. In: American Concrete Institute; Detroit: MI; 1956.
20. ICBO. Uniform building code. In: International Conference of Building Officials; Whittier: CA; 1961.
21. ICBO. Uniform building code, 1927 edition. In: International Conference of Building Officials; Whittier: CA; 1927.
22. ACI. Building code requirements for reinforced concrete (ACI 318–77) and commentary - ACI 318–77C. In: American Concrete Institute; Detroit: MI; 1977.
23. ACI. ACI 318–19 Building code requirements for structural concrete and commentary; In: American Concrete Institute; Detroit: MI; 2019. doi: 10.14359/51716937
24. Standards New Zealand. NZS 3101:2006:A3 - Concrete Structures Standard; 2006.
25. Lynn AC, Moehle JP, Mahin SA, Holmes WT. Seismic evaluation of existing reinforced concrete building columns. *Earthq Spectra*. 1996;12(4):715-739.
26. Elwood KJ, Moehle JP. Axial capacity model for shear-damaged columns. *ACI Struct J*. 2005;102(4):578-587.
27. Cho J, Pincheira JA. Inelastic analysis of reinforced concrete columns with short lap splices subjected to reversed cyclic loads. *ACI Struct J*. 2006;103(2):280-290.
28. Chowdhury SR, Orakcal K. An analytical model for reinforced concrete columns with lap splices. *Eng Struct*. 2012;43:180-193.
29. Girard C, Bastien J. Finite-element bond-slip model for concrete columns under cyclic loads. *J Struct Eng*. 2002;128(12):1502-1510. 128:12(1502).
30. Boys A. Assessment of the seismic performance of inadequately detailed reinforced concrete columns: Master's thesis. In: Department of Civil and Natural Resources Engineering, University of Canterbury. Stanford: CA; 2009.
31. Lignos DG, Krawinkler H. Deterioration modeling of steel components in support of collapse prediction of steel moment frames under earthquake loading. *J Struct Eng*. 2011;137(11):1291-1302.
32. Mazzoni S, McKenna F, Scott MH, Fenves GL. OpenSees command language manual. *Pacific Earthq Eng Res Cent*. 2006;264.
33. Haselton CB, Liel AB, Taylor-Lange SC, Deierlein GG. Calibration of model to simulate response of reinforced concrete beam-columns to collapse. *ACI Struct J*. 2016;113(6):1141-1152.
34. Elwood KJ, MO Eberhard. Effective stiffness of reinforced concrete columns. *ACI Struct J*. 2009;106(4):476-484.
35. Opabola EA, Elwood KJ. Simplified approaches for estimating yield rotation of reinforced concrete beam-column components. *ACI Struct J*. 2020;117(4):279-291.
36. Elwood KJ, Matamoros AB, Wallace JW, et al. Update to ASCE/SEI 41 concrete provisions. *Earthq Spectra*. 2007;23(3):493-523.

37. Opabola EA, Elwood KJ, Oliver S. Deformation capacity of reinforced concrete columns with smooth reinforcement. *Bull Earthq Eng*. 2019;17(5):2509-2532.
38. Rahnama M, Krawinkler H. Effects of soft soil and hysteresis model on seismic demands. Vol 108. In: John A. Blume Earthquake Engineering Center. Stanford: CA; 1993.
39. Lignos D. Sidesway collapse of deteriorating structural systems under seismic excitations: PhD thesis. In: Department of Civil and Environmental Engineering, Stanford University. Stanford: CA; 2008.
40. CEB. *CEB-FIP model code 1990: design code*. In: Comité Euro-International du béton, Fédération Internationale de la Précontrainte, eds. CEB-FIP Model Code 1990: Design Code. London: Thomas Telford Publishing; 1993.
41. Massicotte B, Boucher-Proulx G. Seismic retrofitting of rectangular bridge piers with UHPFRC jackets. In: *BEFIB 2008: 7th RILEM International Symposium on Fibre Reinforced Concrete*. RILEM Publications SARL; 2008:969-975.
42. Elwood KJ. Modelling failures in existing reinforced concrete columns. *Can J Civ Eng*. 2004;31(5):846-859.
43. LeBorgne MR, Ghannoum WM. Calibrated analytical element for lateral-strength degradation of reinforced concrete columns. *Eng Struct*. 2014;81:35-48.
44. Elwood KJ, Moehle JP. Drift capacity of reinforced concrete columns with light transverse reinforcement. *Earthq Spectra*. 2005;21(1):71-89.
45. Harrington CC, Liel AB. Evaluation of seismic performance of reinforced concrete frame buildings with retrofitted columns. *J Struct Eng*. 2020;146(11):4020237.
46. Padgett JE, DesRoches R. Methodology for the development of analytical fragility curves for retrofitted bridges. *Earthq Eng Struct Dyn*. 2008;37(8):1157-1174.
47. Harajli MH, Rteil AA. Effect of confinement using fiber-reinforced polymer or fiber-reinforced concrete on seismic performance of gravity load-designed columns. *Struct J*. 2004;101(1):47-56.
48. Haroun MA, Elsanadedy HM. Fiber-reinforced plastic jackets for ductility enhancement of reinforced concrete bridge columns with poor lap-splice detailing. –. 2005;10(6):749-757.
49. Harries KA, Ricles JR, Pessiki S, Sause R. Seismic retrofit of lap splices in nonductile square columns using carbon fiber-reinforced jackets. *ACI Struct J*. 2006;103(6):874-884.
50. ElGawady M, Endeshaw M, McLean D, Sack R. Retrofitting of rectangular columns with deficient lap splices. *J Compos Constr*. 2010;14(1):22-35.
51. Priestley MJN, Seible F, Calvi GM. *Seismic Design and Retrofit of Bridges*. Hoboken, NJ: Wiley; 1996.
52. Priestley MJN, Calvi GM, Kowalsky MJ. *Displacement – Based Seismic Design of Structures*. Pavia: IUSS Press; 2007.
53. ACI Committee 440. Guide for the design and construction of externally bonded FRP systems for strengthening concrete structures (ACI 440.2 R-17). 2017.
54. Alvarez JC, Brena SF. Non-linear modeling parameters for jacketed columns used in seismic rehabilitation of rc buildings. *Spec Publ*. 2014;297:1-22.
55. Kadysiewski S. *Inventory of Concrete Buildings in San Francisco*. Concrete Coalition; 2010.
56. Blaikie EL, Spurr DD. Earthquake risk associated with 1935 - 1975 Reinforced concrete buildings in NZ. In: Earthquake and War Damage Commission; 1990.
57. Ellingwood B. Development of a probability based load criterion for American National Standard A58: Building code requirements for minimum design loads in buildings and other structures, Vol 13. US Department of Commerce, National Bureau of Standards; 1980.
58. Priestley MJN, Calvi GM. Towards a capacity-design assessment procedure for reinforced concrete frames. *Earthq Spectra*. 1991;7(3):413-437.
59. Shin J, Scott DW, Stewart LK, Yang C-S, Wright TR, DesRoches R. Dynamic response of a full-scale reinforced concrete building frame retrofitted with FRP column jackets. *Eng Struct*. 2016;125:244-253.
60. Baker JW. Conditional mean spectrum: tool for ground-motion selection. *J Struct Eng*. 2011;137(3):322-331.
61. Seible F, Priestley MJN, Hegemier GA, Innamorato D. Seismic retrofit of RC columns with continuous carbon fiber jackets. *J Compos Constr*. 1997;1(2):52-62.
62. Shin YB. *Dynamic Response of Ductile and Non-Ductile Reinforced Concrete Columns*. Berkeley: PhD Thesis. In: Department of Civil and Environmental Engineering, University of California; 2007.
63. Vamvatsikos D, Cornell CA. Incremental dynamic analysis. *Earthq Eng Struct Dyn*. 2002;31(3):491-514.
64. FEMA. Quantification of building seismic performance factors, FEMA P-695. In: Applied Technology Council for the Federal Emergency Management Agency. California: VA; 2009.
65. Wen YK, Ellingwood BR, Bracci JM. Vulnerability function framework for consequence-based engineering, MAE center report 04-04. In: University of Illinois; Champaign: IL; 2004.
66. Celik OC, Ellingwood BR. Seismic fragilities for non-ductile reinforced concrete frames - role of aleatoric and epistemic uncertainties. *Struct Saf*. 2010;32(1):1-12.

How to cite this article: Opabola EA, Elwood KJ, Liel A. Evaluation of seismic performance of as-built and retrofitted reinforced concrete frame structures with LAP splice deficiencies. *Earthquake Engng Struct Dyn*. 2021;50:3138–3159. https://doi.org/10.1002/eqe.3503